



This is the accepted manuscript made available via CHORUS. The article has been published as:

Controlling Local Thermalization Dynamics in a Floquet-Engineered Dipolar Ensemble

Leigh S. Martin, Hengyun Zhou, Nathaniel T. Leitaο, Nishad Maskara, Oksana Makarova, Haoyang Gao, Qian-Ze Zhu, Mincheol Park, Matthew Tyler, Hongkun Park, Soonwon Choi, and Mikhail D. Lukin

Phys. Rev. Lett. **130**, 210403 — Published 25 May 2023

DOI: [10.1103/PhysRevLett.130.210403](https://doi.org/10.1103/PhysRevLett.130.210403)

Controlling Local Thermalization Dynamics in a Floquet-Engineered Dipolar Ensemble

Leigh S. Martin^{1,*}, Hengyun Zhou^{1,*,†}, Nathaniel T. Leita^{1,*}, Nishad Maskara¹, Oksana Makarova^{1,2}, Haoyang Gao¹, Qian-Ze Zhu^{1,2}, Mincheol Park¹, Matthew Tyler¹, Hongkun Park^{1,3}, Soonwon Choi⁴, Mikhail D. Lukin^{1,†}

¹Department of Physics, Harvard University, Cambridge, Massachusetts 02138, USA

²School of Engineering and Applied Sciences, Harvard University, Cambridge, Massachusetts 02138, USA

³Department of Chemistry and Chemical Biology, Harvard University, Cambridge, Massachusetts 02138, USA

⁴Center for Theoretical Physics, Massachusetts Institute of Technology, Cambridge, Massachusetts 02139, USA

*These authors contributed equally to this work.

†To whom correspondence should be addressed; E-mail: hzhou@g.harvard.edu, lukin@physics.harvard.edu

Understanding the microscopic mechanisms of thermalization in closed quantum systems is among the key challenges in modern quantum many-body physics. We demonstrate a method to probe local thermalization in a large-scale many-body system by exploiting its inherent disorder, and use this to uncover the thermalization mechanisms in a three-dimensional, dipolar-interacting spin system with tunable interactions. Utilizing advanced Hamiltonian engineering techniques to explore a range of spin Hamiltonians, we observe a striking change in the characteristic shape and timescale of local correlation decay as we vary the engineered exchange anisotropy. We show that these observations originate from the system's intrinsic many-body dynamics and reveal the signatures of conservation laws within localized clusters of spins, which do not readily manifest using global probes. Our method provides an exquisite lens into the tunable nature of local thermalization dynamics, and enables detailed studies of scrambling, thermalization and hydrodynamics in strongly-interacting quantum systems.

Thermalization in isolated quantum many-body systems underlies the emergence of quantum statistical mechanics. This happens despite the unitary, reversible evolution of a closed quantum system, and is commonly understood from the perspective of the system acting as its own bath, as formalized by the eigenstate thermalization hypothesis [1–8]. Equally important is the dynamics by which a system reaches thermal equilibrium. Recent work has uncovered various universal phenomena, including scrambling [9–11] and hydrodynamic transport [12–15]. However, many aspects of this approach to thermal equilibrium are still poorly understood, particularly in regards to how thermalizing dynamics and the eigenstate thermalization hypothesis emerge from coherent interactions within a closed system.

In this Letter, we demonstrate a new tool to probe local dynamics in strongly-interacting systems without the need for single-spin control or readout. We apply it to the paradigmatic XXZ model in a positionally disordered, dipolar spin system, in which the nanometer-scale spin-spin separation and three-dimensional geometry make single-site operations infeasible. Combining this method with advanced Hamiltonian engineering pulse sequences [7, 16–19], we transform the native system Hamiltonian into a wide range of XXZ Hamiltonians and access qualitatively distinct regimes of equilibration. We find that the local thermalization dynamics are consistent with coherently coupled clusters of spins that interact with each other via fluctuating magnetic fields, whose correlation times and hybridization determine the timescale and shape of the decay. Our method provides a powerful lens into the tunable nature of local relaxation dynamics in closed quantum many-body systems, which is not accessible via global Ramsey probes [19].

Experimental system and Hamiltonian engineering.— Our experimental system (Fig. 1(a)) consists of a high density

(~15 ppm), positionally-disordered ensemble of negatively-charged nitrogen-vacancy (NV) centers in diamond [20]. The NV center spin in its electronic ground state forms a spin-1 triplet, from which we isolate a spin-1/2 degree of freedom via the application of an external magnetic field aligned with one group of NVs with the same lattice orientation. The high density of NV centers enables strong, dipolar interactions between nearby spins ($J \approx (2\pi)35$ kHz at a typical separation). Additional paramagnetic defects and lattice strain result in large on-site disorder ($W \approx (2\pi)4$ MHz) of the spins. Green laser illumination enables optical polarization of the spin state, while fluorescence on the red phonon sideband allows read out of the final global spin polarization. Microwave pulses resonant with the target NV spin transition frequency allow fast manipulation of the spin state and Hamiltonian engineering (see Ref. [6, 21, 22] for experimental details).

We utilize an improved version [23] of the robust Hamiltonian engineering techniques (Fig. 1(b,c)) introduced in Ref. [16] to suppress local disorder and engineer tunable XYZ spin-spin interaction Hamiltonians

$$H_{\mathbf{g}} = \sum_{ij} J_{ij} (g_x S_i^x S_j^x + g_y S_i^y S_j^y + g_z S_i^z S_j^z), \quad (1)$$

parameterized by an anisotropy vector, $\mathbf{g} = (g_x, g_y, g_z)$. This is accomplished by tuning the evolution time along each of the three axis directions (Fig. 1(b,c)). Here, $J_{ij} \propto 1/r_{ij}^3$ is the long-ranged, anisotropic dipolar interaction strength. We primarily focus on XXZ Hamiltonians, where we parameterize the interaction as $\mathbf{g}(\lambda_{\text{XXZ}}) = (1 + \lambda_{\text{XXZ}}, 1 + \lambda_{\text{XXZ}}, 1 - 2\lambda_{\text{XXZ}})/3$ with λ_{XXZ} characterizing the distance away from the $SU(2)$ symmetric Heisenberg Hamiltonian, see Fig. 1(d). Although our main pulse sequence cannot engineer the Ising point $\mathbf{g} = (0, 0, 1)$ due to finite-pulse effects, we use a spin locking sequence (i.e. con-

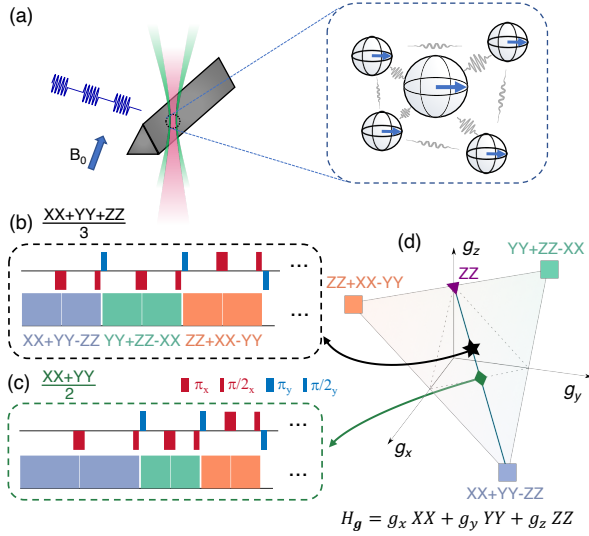


FIG. 1. Experimental system and Hamiltonian engineering. (a) Black diamond experimental system, consisting of a high density ensemble of NV spins in diamond. Spin initialization and readout are achieved via optical illumination and fluorescence, while spin manipulation is performed via microwave pulses. (b,c) Representative pulse sequence block and illustration of Hamiltonian engineering concept. By tuning pulse separations in an interaction decoupling sequence, the effective Hamiltonian can be engineered into different forms, such as Heisenberg (b) or XY (c) Hamiltonians. (d) Illustration of accessible XYZ Hamiltonians via Hamiltonian engineering. The accessible Hamiltonians are averages of those obtained via transforming the native Hamiltonian by a $\pi/2$ pulse [squares]. Special Hamiltonians of interest are labeled: Ising [purple triangle], Heisenberg [black star], XY Hamiltonian [green diamond].

tinuous driving) to access it.

Global and local probes of thermalization.— Equipped with the ability to engineer various XXZ Hamiltonians, we now explore the thermalization dynamics. We first examine the dynamics of global observables, utilizing a conventional Ramsey sequence to measure the decay of a polarized initial state along $+\hat{x}$ [24], given by

$$\mathcal{C}_{\text{Global}}^{XX}(t) = \frac{2}{N} \langle S^x(t) \rangle_{+\hat{x}} = \left(\frac{2}{N} \right)^2 \langle S^x(t) S^x(0) \rangle_{+\hat{x}}, \quad (2)$$

where $S^\mu(t) = \sum_i S_i^\mu(t) = \sum_i e^{iH_\theta t} S_i^\mu e^{-iH_\theta t}$ is the Heisenberg picture *global* spin operator and $\langle \cdot \rangle_{+\hat{x}}$ denotes an ensemble average in the state where all spins are initially polarized along the $+\hat{x}$ direction.

As a validation of our Hamiltonian engineering tools, we first engineer the Heisenberg Hamiltonian $\lambda_{XXZ} = 0$, which exhibits a global SU(2) symmetry and therefore preserves uniformly polarized initial states. As seen in Fig. 2(a), global Heisenberg dynamics display an order of magnitude longer decay timescale than the disorder-decoupled native NV interaction Hamiltonian (gray points). To characterize the timescale and shape of the decay, we fit the signal to a stretched exponential form $\mathcal{C}(t) \propto \exp(-(t/\tau)^\nu)$, where τ

describes the characteristic timescale, and the stretching exponent ν encodes the shape (solid lines in Fig. 2(a)). In Fig. 2(b), the blue points show the decay timescale for a range of different XXZ Hamiltonians, normalized by the decay curve at the Heisenberg Hamiltonian, which is completely dominated by extrinsic factors. Conversely, the prominent peak around the Heisenberg Hamiltonian confirms that the normalized decay is dominated by dynamics of the engineered Hamiltonian.

While the Heisenberg Hamiltonian freezes the decay of any polarized initial state, it still induces dynamics in generic initial states, leading to local thermalization. To probe this local equilibration for generic initial states, we introduce a technique to measure the infinite temperature *local* spin autocorrelators, despite only having access to native *global* control and measurements, by leveraging the inherent large disorder of the system. We refer to this probe as a “disorder-order” measurement [25]. It prepares the spins in a random product state encoding the local disorder strength on each spin to mimic an infinite temperature quench.

The measurement sequence is illustrated in Fig. 2(c), and resembles the familiar spin-echo technique. The disorder-winding and unwinding free evolutions surrounding the Floquet Hamiltonian engineering serve two essential purposes. First, the initial free-evolution step distributes each spin uniformly along the equator of its Bloch sphere, with the disorder field h_i imprinting a local phase $\theta_i = h_i \tau_{\text{wind}}$. This step initializes a random product state at infinite effective temperature. Second, reversing the initial disorder-winding prior to measurement of global polarization transforms the spatially homogeneous measurement of the ensemble into a spatially inhomogeneous measurement, where each spin is locally measured along the direction in which they were initially prepared. This local realignment (see Fig. 2(d)) allows only the local operator autocorrelations associated to the plane of the disorder-winding to survive the disorder average. The resulting signal is

$$\frac{2}{N} \sum_i \langle S_i^x(t) S_i^x(0) \rangle_{T=\infty} + \langle S_i^y(t) S_i^y(0) \rangle_{T=\infty}, \quad (3)$$

where $\langle \cdot \rangle_{T=\infty}$ denotes an expectation value over the infinite temperature state [21].

Note that despite their superficial similarities, Eq. (3) is very different from Eq. (2); for example, a Heisenberg Hamiltonian does not cause any decay in Eq. (2), but does cause local equilibration in Eq. (3). We further generalize this protocol for disordered rotations around the \hat{x} , \hat{y} , \hat{z} axes and combine the results to infer the local autocorrelations of each axis individually, *i.e.* $\mathcal{C}_{\text{Local}}^{\mu\mu}(t) = \frac{4}{N} \sum_i \langle S_i^\mu(t) S_i^\mu(0) \rangle_{T=\infty}$ for $\mu = X, Y, Z$.

The decay timescales for the disorder-order measurements are shown as the red traces in Fig. 2. In Fig. 2(a,b), we find that the decay of such local correlators for the Heisenberg Hamiltonian is significantly faster than the global correlators, confirming that the disorder-order technique detects local thermalization, even in the SU(2)-symmetric case that preserves polarized initial states.

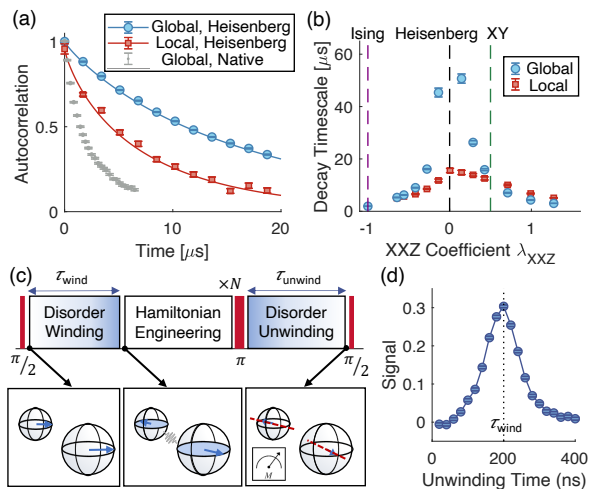


FIG. 2. Measuring global and local spin autocorrelators. (a) Measured coherence decay under an engineered Heisenberg Hamiltonian for global [blue circles] and local [red squares] spin autocorrelators. Fit is a stretched exponential. For reference, we also show the XY-8 decay [gray points], which characterizes the decay under the native interaction Hamiltonian. (b) Decay times for normalized global and local spin autocorrelators. Vertical dashed lines denote special Hamiltonians of interest. (c) “Disorder Order” sequence to measure the decay of local spin autocorrelators for an infinite temperature initial state, which reveals local thermalization. The sequence consists of a $\pi/2$ initialization pulse, a free evolution duration to encode the local disorder strength into the spin state, a varying number of repetitions of the Hamiltonian engineering sequence, followed by a π pulse and free evolution to rephase the spins and $-\pi/2$ pulse for spin state readout. The sequence is designed to suppress higher-order corrections (see Ref. [21] for details). (d) Measured normalized spin polarization as a function of disorder unwinding time, showing a revival when the winding and unwinding times are equal. In this example, the Hamiltonian engineering consists of two Floquet cycles of Heisenberg Hamiltonian engineering.

Tuning local thermalization.— Interestingly, different XXZ Hamiltonians show markedly different decay shapes, as shown in Fig. 3(b). Varying the XXZ Hamiltonian for local spin autocorrelators along X, we find a significant deviation of the decay shape from a simple exponential form, contrary to conventional NMR heuristics [26]. While the simple exponential shape qualitatively captures features close to the Ising Hamiltonian, we observe a striking decrease of the stretching exponent on the easy-plane side of the phase diagram ($\lambda_{XXZ} > 0$), where $|g_{x,y}| > |g_z|$. As we will see, the unexpected variations of the stretching exponent are an explicit manifestation of the intrinsic, quantum many-body noise being tuned by the effective Hamiltonian.

To provide a physical explanation for the observed decay timescales and shapes, we develop a simple physical model and complement it with numerical simulations that qualitatively reproduce the observations.

Focusing first on the decay shape of the engineered Ising dynamics, one can analytically calculate the global and lo-

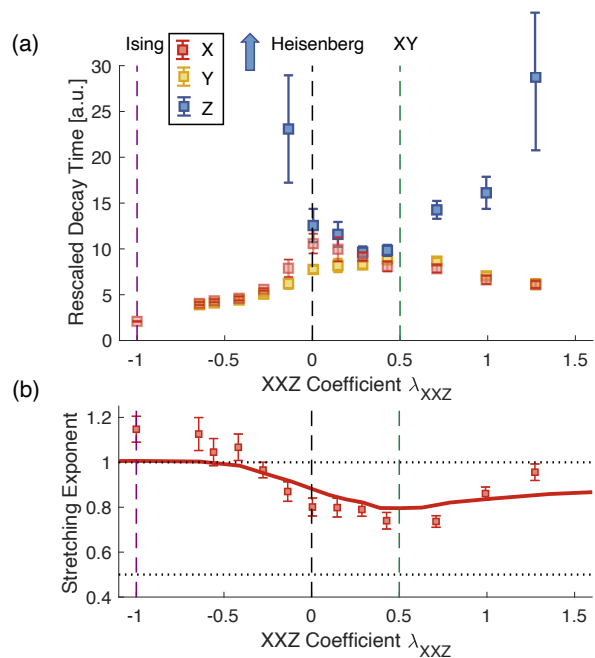


FIG. 3. Decay timescale and decay shape for local correlators. (a) Local X [red], Y [yellow] and Z [blue] spin autocorrelator decay timescales, normalized by extrinsic decay and rescaled by Hamiltonian norm. The blue arrow indicates divergent timescales of Z correlators closer to the Ising Hamiltonian [21]. (b) Local spin autocorrelator decay shapes, averaged over X, Y, as characterized by the stretching exponent. Horizontal dotted line at $d/\alpha = 1$ is the naive expectation based on existing arguments in the NMR literature, predicting an exponential decay. A second dashed line at $0.5 = d/2\alpha$ is also plotted as the expectation for dynamics which generate Markovian fluctuating fields. Solid line is the prediction from a dynamical mean-field model.

cal S_x autocorrelators for randomly-positioned d -dimensional spin ensembles with power-law $1/r^\alpha$ Ising interactions [27–29]. For any given spin, quantum fluctuations of neighboring spins produce a random magnetic field $\hat{B}_i = \sum_j J_{ij} \hat{S}_j^z$ driving precession dynamics in the XY plane. Crucially, this magnetic field is static, as the local magnetization S_j^z is conserved under the ZZ Ising Hamiltonian, and spins precess ballistically as $\Delta\phi_t(r) \sim t/r^\alpha$. Counting the number of spins contributing to this precession, as depicted in Fig. 4(a), leads to a stretching exponent of d/α , in agreement with our experimental observations.

Away from the Ising Hamiltonian, the non-zero flip-flop term $g_{x,y}$ transports magnetization through the spin bath, rendering the local field dynamical. When the correlation time of the field becomes comparable to the precession timescale, the accrued phases can destructively interfere. This qualitatively modifies the earlier scaling to $\Delta\phi_t(r) \sim t^\beta/r^\alpha$, where $1 \geq \beta \geq 1/2$ is a phenomenological parameter interpolating between ballistic and diffusive precession dynamics in the respective limits of static and Markovian fields, see Fig. 4(b). Shorter bath correlation times reduce the stretching exponent

to $\nu = \beta d/\alpha$, and yield $d/2\alpha$ in the Markovian limit.

To confirm that the bath correlation times determine the stretching exponents in the full non-commuting XXZ Hamiltonian, we use a minimal model that incorporates the correlation times and vector nature of the dynamic magnetic field into a self-consistent dynamical mean-field model [21, 30]. In particular, we approximate the quantum magnetic fields by zero-mean, normally distributed classical variables whose temporal correlations are self-consistently determined by the local dephasing dynamics of neighbouring spins. The resulting decay shapes and stretching exponents qualitatively match the experimental data (red line in Fig. 3(b)), validating our intuition that dynamic magnetic fields transverse to a particular spin axis produce lower stretching exponents than static ones.

The above physical picture explains the easy-axis regime timescales, but not the easy plane. On the easy-axis side, the static Z fields lead to rapid, linear accumulation of precession phase, which causes rapid decay of the X and Y correlation functions. This prediction agrees with the $\lambda_{XXZ} < 0$ region of Fig. 3(b), where the ratio of X to Z timescales (plotted in Fig. 4(e)) remains below 1. However on the easy plane side, and in particular for the XY point $H \propto S^x S^x + S^y S^y$, we would expect Z fields to decay faster than X and Y fields, and therefore the X to Z timescale ratio to significantly exceed 1, simply because there are more fields transverse to it. This runs contrary to observation, as can be clearly seen in the $\lambda_{XXZ} > 0$ region of Fig. 3(b) and Fig. 4(e). Figure 4(e) also shows the expectation from the single-spin dynamical mean-field model, which shows sizable deviations from experimental observations.

To address these discrepancies, we consider a model including exact coherent interactions between strongly coupled pairs of spins within the dynamical mean field framework, as is depicted schematically in Fig. 4(d) and compared against data in Fig. 4(e). This improvement can be understood by noting that local conservation of magnetization within these clusters significantly extends the Z decay timescale relative to the transverse axes. Thus, the reduction of the peak in timescale ratio near the XY Hamiltonian constitutes a signature of hybridization of clusters of spins contributing to the thermalization dynamics. It is noteworthy that both experiment and exact diagonalization (Fig. 4(e)) give a lower timescale ratio than the pair-spin model, suggesting that the experiment witnesses quantum correlations that go beyond two-body clusters.

Discussions.— These observations reveal the interplay between coherent hybridization and local dephasing as a concrete thermalization mechanism in a closed many-body system, and open up a wide range of opportunities for explorations in many-body physics and quantum sensing. The disorder-order technique allows us to probe complex many-body phenomena where local control is otherwise inaccessible. It will also be interesting to extend the Hamiltonian engineering techniques to higher spin dimensions, utilizing the full spin-1 nature of the NV center spin to access a richer range of dynamical phenomena [31, 32], or to extend the measurement techniques for local autocorrelations to more intricate spin

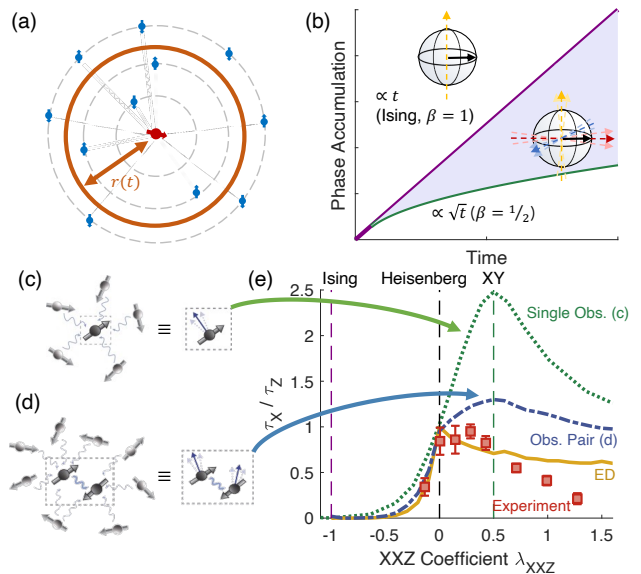


FIG. 4. **Physical mechanism driving coherence decay.** (a) Quantum fluctuations of neighboring spins produce a dynamical mean-field that induces decay, and as time progresses, weakly coupled spins at larger distances start to contribute as well. (b) For different Hamiltonians, the correlation time of the dynamical mean-field changes, resulting in different rates of phase accumulation over time (ballistic for a static field, diffusive for a Markovian fast-varying field) and leading to different decay shapes at early-to-intermediate times. (c) Illustration of a single spin experiencing the fluctuating magnetic field from its neighbors. (d) Illustration of the additional effect of hybridization between strongly coupled pairs of spins. (e) Ratio between X and Z decay times of local correlators for experimental data and various models. Including local hybridization [blue] improves the agreement with experimental data [red], and exact diagonalization of full quantum dynamics [yellow, 18 spins] agrees best.

correlators, such as out-of-time-ordered-correlators [7, 33]. Finally, our results highlight the ability to engineer complex interaction Hamiltonians and probe the resulting evolution, a key building block towards the use of such solid-state ensemble spin systems for entanglement-enhanced quantum sensing [34–36]. The techniques demonstrated here should be applicable to a wide variety of quantum simulation and sensing platforms.

Acknowledgements.— We thank Yimu Bao, Paola Cappellaro, Joonhee Choi, Jordan Cotler, Eugene Demler, Wen Wei Ho, Francisco Machado, Daniel Parker, Pai Peng, Alex Schuckert, Norman Yao, Bingtian Ye, Bihui Zhu and Chong Zu for helpful conversations. We also thank Junichi Isoya, Shinobu Onoda, Hitoshi Sumiya and Fedor Jelezko for providing the black diamond sample. This work was supported in part by CUA, HQI, Vannevar Bush Faculty Fellowship Program, ARO MURI, DARPA DRINQS, Moore Foundation GBMF-4306.

Note added: after the completion of this project, we became aware of related work [40], which develops similar techniques

and applies them to study spin transport.

-
- [1] L. D’Alessio, Y. Kafri, A. Polkovnikov, and M. Rigol, *Advances in Physics* **65**, 239 (2016).
- [2] D. A. Abanin, E. Altman, I. Bloch, and M. Serbyn, *Reviews of Modern Physics* **91**, 021001 (2019).
- [3] T. Langen, S. Erne, R. Geiger, B. Rauer, T. Schweigler, M. Kuhnert, W. Rohringer, I. E. Mazets, T. Gasenzer, and J. Schmiedmayer, *Science* **348**, 207 (2015).
- [4] M. Schreiber, S. S. Hodgman, P. Bordia, H. P. Lüschen, M. H. Fischer, R. Vosk, E. Altman, U. Schneider, and I. Bloch, *Science* **349**, 842 (2015).
- [5] A. M. Kaufman, M. E. Tai, A. Lukin, M. Rispoli, R. Schittko, P. M. Preiss, and M. Greiner, *Science* **353**, 794 (2016).
- [6] G. Kucsko, S. Choi, J. Choi, P. C. Maurer, H. Zhou, R. Landig, H. Sumiya, S. Onoda, J. Isoya, F. Jelezko, E. Demler, N. Y. Yao, and M. D. Lukin, *Physical Review Letters* **121**, 023601 (2018).
- [7] K. X. Wei, C. Ramanathan, and P. Cappellaro, *Physical Review Letters* **120**, 070501 (2018).
- [8] J. Choi, H. Zhou, S. Choi, R. Landig, W. W. Ho, J. Isoya, F. Jelezko, S. Onoda, H. Sumiya, D. A. Abanin, and M. D. Lukin, *Physical Review Letters* **122**, 043603 (2019).
- [9] P. Hayden and J. Preskill, *Journal of High Energy Physics* **2007**, 120 (2007).
- [10] S. H. Shenker and D. Stanford, *Journal of High Energy Physics* **2014**, 67 (2014).
- [11] K. A. Landsman, C. Figgatt, T. Schuster, N. M. Linke, B. Yoshida, N. Y. Yao, and C. Monroe, *Nature* **567**, 61 (2019).
- [12] K. X. Wei, E. Magesan, I. Lauer, S. Srinivasan, D. F. Bogorin, S. Carnevale, G. A. Keefe, Y. Kim, D. Klaus, W. Landers, N. Sundaresan, C. Wang, E. J. Zhang, M. Steffen, O. E. Dial, D. C. McKay, and A. Kandala, *arXiv preprint arXiv:2106.00675* (2021).
- [13] P. N. Jepsen, J. Amato-Grill, I. Dimitrova, W. W. Ho, E. Demler, and W. Ketterle, *Nature* **588**, 403 (2020).
- [14] C. Zu, F. Machado, B. Ye, S. Choi, B. Kobrin, T. Mittiga, S. Hsieh, P. Bhattacharyya, M. Markham, D. Twitchen, A. Jarmola, D. Budker, C. R. Laumann, J. E. Moore, and N. Y. Yao, *Nature* **597**, 45 (2021).
- [15] V. B. Bulchandani, S. Gopalakrishnan, and E. Ilievski, *Journal of Statistical Mechanics: Theory and Experiment* **2021**, 084001 (2021).
- [16] J. Choi, H. Zhou, H. S. Knowles, R. Landig, S. Choi, and M. D. Lukin, *Physical Review X* **10**, 031002 (2020).
- [17] H. Zhou, L. S. Martin, M. Tyler, O. Makarova, N. Leitao, H. Park, and M. D. Lukin, *arXiv preprint arXiv:2303.07363* (2023).
- [18] M. Tyler, H. Zhou, L. S. Martin, N. Leitao, and M. D. Lukin, *arXiv preprint arXiv:2303.07374* (2023).
- [19] S. Geier, N. Thaicharoen, C. Hainaut, T. Franz, A. Salzinger, A. Tebben, D. Grimshandl, G. Zürn, and M. Weidemüller, *Science* **374**, 1149 (2021).
- [20] M. W. Doherty, N. B. Manson, P. Delaney, F. Jelezko, J. Wrachtrup, and L. C. Hollenberg, *Physics Reports* **528**, 1 (2013).
- [21] See Supplemental Material for more details on the experimental setup, numerical simulations and theoretical models, which also includes Refs. [37-39].
- [22] H. Zhou, J. Choi, S. Choi, R. Landig, A. M. Douglas, J. Isoya, F. Jelezko, S. Onoda, H. Sumiya, P. Cappellaro, H. S. Knowles, H. Park, and M. D. Lukin, *Physical Review X* **10**, 031003 (2020).
- [23] H. Zhou et al., in preparation.
- [24] R. Nandkishore and S. Gopalakrishnan, *Physical Review B* **103** (2021), 10.1103/PhysRevB.103.134423.
- [25] J. Jeener and P. Broekaert, *Physical Review* **157**, 232 (1967).
- [26] A. Abragam, *The principles of nuclear magnetism* (Oxford university press, 1961).
- [27] E. B. Fel’dman and S. Lacelle, *Journal of Chemical Physics* **104**, 2000 (1996).
- [28] E. J. Davis, B. Ye, F. Machado, S. A. Meynell, T. Mittiga, W. Schenken, M. Joos, B. Kobrin, Y. Lyu, D. Bluvstein, S. Choi, C. Zu, A. C. B. Jayich, and N. Y. Yao, *arXiv preprint arXiv:2103.12742* (2021).
- [29] B. L. Dwyer, L. V. H. Rodgers, E. K. Urbach, D. Bluvstein, S. Sangtawesin, H. Zhou, Y. Nassab, M. Fitzpatrick, Z. Yuan, K. De Greve, E. L. Peterson, J.-P. Chou, A. Gali, V. V. Dobrovitski, M. D. Lukin, and N. P. de Leon, *PRX Quantum* **3**, 040328 (2021).
- [30] T. Gräßer, P. Bleicker, D. B. Hering, M. Yarmohammadi, and G. S. Uhrig, *Physical Review Research* **3**, 043168 (2021).
- [31] S. Choi, N. Y. Yao, and M. D. Lukin, *Physical Review Letters* **119**, 183603 (2017).
- [32] M. Schechter and T. Iadecola, *Physical Review Letters* **123**, 147201 (2019).
- [33] M. Garttner, J. G. Bohnet, A. Safavi-Naini, M. L. Wall, J. J. Bollinger, and A. M. Rey, *Nature Physics* **13**, 781 (2017).
- [34] E. Davis, G. Bentsen, and M. Schleier-Smith, *Physical Review Letters* **116**, 053601 (2016).
- [35] O. Hosten, R. Krishnakumar, N. J. Engelsen, and M. A. Kasevich, *Science* **352**, 1552 (2016).
- [36] P. Cappellaro and M. D. Lukin, *Physical Review A* **80**, 032311 (2009).
- [37] J. Schachenmayer, A. Pikovski, and A. M. Rey, *Physical Review X* **5**, 011022 (2015).
- [38] S. Sachdev and J. Ye, *Physical Review Letters* **70**, 3339 (1993).
- [39] T. G. Zhou, L. Pan, Y. Chen, P. Zhang, and H. Zhai, *Physical Review Research* **3**, L022024 (2021).
- [40] P. Peng, B. Ye, N. Y. Yao, and P. Cappellaro, *Nature Physics* **2023**, 1 (2023).